# Applying Malawi Continuously Operating Reference Stations (CORS) in GNSS Meteorology

Robert Galatiya Suya[1], Charles Chisha Kapachika[2], Mphatso Oscar Soko[3], Vincent Luhanga[4], John Bosco Ogwang[5], Harvey Chilembwe[6], Francis Gitau[7]

[1, 2, 3, 4] Department of Land Surveying, School of the Built Environment, Malawi University of Business and Applied Sciences, Private Bag 303, Chichiri, Blantyre, Malawi

[5] Institute of Survey and Land Management, Po Box 89, Entebbe, Kampala, Uganda

[6] Department of Geography and Earth Sciences Faculty of Science, University of Malawi, P.O BOX 280, Zomba, Malawi

[7] School of Mines and Engineering, Taita Taveta University, P.O Box 635-80300 Voi, Kenya

DOI: http://dx.doi.org/10.4314/sajg.v11i2.4

## Abstract

*Global Navigation Satellite System (GNSS) signals in the L-band are affected by the non-dispersive neutral atmosphere. Regardless of their center frequency, the L-band code and phase observations are affected by the same measure of delay. GNSS receivers play a significant role in quantifying the zenith tropospheric delay (ZTD) from satellite signals. Malawi has a Continuously Operating Reference Stations (CORS) network which was established to support research in geophysical geodesy and geodynamics. However, the quality of the observations tracked by the CORS has never been tested in terms of its meteorological application. In this paper, the ZTD estimation approach and the evaluation of results from the Global Positioning System (GPS) measurements are presented. The optimal approach of precise point positioning (PPP) was used to estimate ZTD from one-week datasets which were collected from six CORS monuments distributed in the northern and southern regions of Malawi. In addition, the zenith wet delay (ZWD) and zenith hydrostatic delay (ZHD) were also estimated to determine their respective contributions to the total delay in all the stations. Alongside the meteorological parameters, the positioning repeatabilities were also established for all stations. Results indicate that the averaged ZTD, ZWD and ZHD can reach as high as 247mm, 47 mm, and 199 mm, respectively. The minimum ZTD, ZWD, and ZHD for the stations can drop to as low as 220 mm, 24 mm, and 181 mm, respectively. This indicates that the ZHD contributes to more than 90% of the total delay at the stations. For the positioning performance, there was no obvious disparity in the latitude (less than 0.5 cm), longitude (less than 1 cm), and ellipsoidal height*

*repeatabilities (less than 1.5 cm). Thus, the results clearly demonstrate that the Malawi CORS network may be used for GNSS-based meteorological applications using the available geodetic receivers. However, for high precision meteorological applications, Malawi may consider densifying the available network with geodetic grade receivers.*

***Keywords:*** *CORS, GNSS Meteorology, Precise Point Positioning; Zenith Tropospheric Delay, Zenith Hydrostatic Delay; Zenith Wet Delay*

## 1. Introduction

Global Navigation Satellite System (GNSS), which comprises Global Positioning System (GPS, for the USA); Global'naya Navigatsionnaya Sputnikova Sistema (GLONASS or Russian Global Navigation Satellite System); BeiDou Navigation Satellite System (BDS, for China), and Galileo (for Europe), has revolutionized positioning, navigation, and timing (PNT) services. Other than PNT applications, GNSS has also extended its roles in meteorology (Gutman and Benjamin, 2001; Shoji, 2009; Kiyani et al., 2020) and weather studies (Gutman et al., 2004; Rahimi, Mohd Shafri and Norman, 2018).

In GNSS meteorology, satellite observations can be tracked with low-cost receivers such as smartphones with a single frequency (Pesyna et al., 2014; Krietemeyer et al., 2018) and a multi-frequency (Paziewski, 2020; Uradziński and Bakuła, 2020) tracking capability. These gadgets act as an alternative to employing reference stations, such as the International GNSS Service (IGS) or the Multi-GNSS Experiment (MGEX) stations, established by agencies, institutions, or countries. In their geographical positions, the stations may be installed alone or co-located with other space geodetic techniques such as Very Long Baseline Interferometry (VLBI); Satellite Laser Ranging (SLR); Doppler Orbitography and Radiopositioning Integrated by Satellite (DORIS); water vapour radiometers (WVR) or tide gauge stations. In both single and multi-purpose CORS networks, ZTDs can be estimated from the tracked GNSS (Bevis et al., 1992; Alshawaf et al., 2017), VLBI (Heinkelmann et al., 2007; Balidakis et al., 2018); SLR (Pollet et al., 2014); DORIS (Teke et al., 2013), and WVR (Bock et al., 2010) observations.

The estimated ZTD is a sum of the components including the zenith wet delay (ZWD) and the zenith hydrostatic delay (ZHD). The ZWD is directly related to ground pressure within the spatial region, whereas the ZHD is linked to the amount of water vapour in the atmosphere. The troposphere, being the first layer of the atmosphere, is influenced by the total refractivity, which is a function of temperature, pressure, and water vapour partial pressure (Essen and Froome, 1951). Furthermore, the quantity of precipitable water can be determined from the available water vapour in the atmosphere which tends to be proportional to ZWD (Hurter and Maier, 2013).

The measurement and monitoring of physical variables such as pressure, temperature, and humidity using GNSS signals is of profound significance to regional and short-term weather forecasting (Awange, 2011). On the

other hand, the existing CORS networks need to accommodate a considerable density of stations to achieve ZTD of improved spatial resolution (Zhao et al., 2018). ZTDs have commonly been estimated from phase observables (Bevis et al., 1992) or combined code and phase (Ahmed et al., 2016; Zhao et al., 2018). As a consequence, ZTD estimates are derived from double differences (DD) or precise point positioning (PPP) techniques (Zumberge et al., 1997). The resultant ZTDs derived from PPP are consistent with the global reference system implied by the fixed global GNSS ephemerides. On the other hand, ZTDs estimated from the DD technique are biased by a datum offset depending on the baseline lengths in the CORS network.

Malawi has a local CORS network purposefully established to support geophysical and geodynamics studies (Shillington et al., 2016). The studies rely on a limited number of CORS monuments, the majority (91%) of which are geographically located in the northern part of the country. While the Malawi CORS network offers such research benefits, the possibility of using the existing CORS monuments in GNSS meteorology has been overlooked. In GNSS meteorology, PPP is one of the optimal techniques requiring only a single geodetic receiver to estimate meteorological parameters. Taking advantage of such a versatile approach, ZTD, ZHD, and ZWD are estimated for the CORS network in Malawi for ten days in this paper. This is achieved not only to demonstrate the feasibility of using Malawi's CORS network in the estimation of meteorological parameters, but also to establish the overall positioning repeatability performance for the individual stations.

## 2. Estimation of Meteorological Parameters

### 2.1. The PPP Technique

As the GNSS signal propagates through the atmosphere, it is delayed by the ionosphere. Typically, GNSS dual-frequency phase and code observables are combined to eliminate first-order ionospheric propagation delays. Hence, the ionosphere-free (IF) combinations of the dual-frequency GPS phase and code observations between satellite $s$ and receiver $r$ can be formulated as in Leick et al.(2015):

$$\left.\begin{aligned} \varphi_{r,f}^{s} &= \rho_r^s + \Delta t_r^s + m_f . ZTD_r^s + M_{r,f}^s + \lambda_{\varphi,f} N_{r,f}^s + \epsilon_r^s \\ P_{r,f}^{s} &= \rho_r^s + \Delta t_r^s + m_f . ZTD_r^s + M_{r,f}^s + \varepsilon_r^s \end{aligned}\right\} \qquad [3.1]$$

with

$$\left.\begin{aligned} \Delta t_r^s &= c(\delta t_r - \delta t^s) \\ \rho_r^s \equiv \| \mathbf{x}^s - \mathbf{x}_r \| &= \| (x^s, y^s, z^s)^T - (x_r, y_r, z_r)^T \| \end{aligned}\right\} \quad [3.2]$$

where $\varphi_{r,f}^s$ denotes the IF phase combination between GPS signals such that $f$ = L1 and L2 signal frequencies; $P_{r,f}^s$ denotes the IF code combination between GPS L1 and L2 signals; $\rho_r^s$ denotes the geometrical range between $s$ and $r$ such that $(x^s, y^s, z^s)$ is the satellite position whereas $(x_r, y_r, z_r)$ is the receiver position; $\Delta t_r^s$ denotes the satellite $(\delta t^s)$ and receiver $(\delta t_r)$ clock offset from the GNSS time; $c$ denotes the vacuum speed of light; $ZTD_r^s$ denotes the signal path delay due to the neutral atmosphere (troposphere). Here, it is worth noting that the unknown wet part of the tropospheric delay is expressed as a product of the ZTD and a mapping function $(m_f)$ relating to the zenith delay; $M_{r,f}^s$ denotes the multipath; $\lambda_{\varphi,f}$ denotes the IF combination of the carrier-phase wavelengths; $N_{r,f}^s$ denotes the non-integer ambiguity of the IF phase combination; and $\epsilon_r^s$ and $\varepsilon_r^s$ denote the phase and code residuals, respectively.

From [3.1], the satellite coordinates and clocks can be fixed by applying the precise GNSS orbits and clock parameters. Thus, the estimable parameters for [3.1] are the receiver position coordinates, which are also the CORS geographical positions $(x_r, y_r, z_r)$ in this paper; the CORS receiver clocks $(\delta t_r)$; ZTD and the float IF phase ambiguities $(N_{r,f}^s)$. Applying least squares or Kalman filter approaches, the estimated parameters $R$ can be expressed as

$$R = \left[x_r, y_r, z_r, \delta t_r, ZTD, N_{r,f}^s\right] \quad [3.3]$$

## 2.2. Estimation of Water Vapour from GPS Observations

In GNSS meteorology, the ZTD expressed in [3.3] can either be assimilated into numerical weather models or be converted to precipitable water vapour (PWV) using surface pressure models. As indicated by Hurter and Maier (2013), the conversion of ZTD into PWV can be achieved using simple atmospheric models. The satellite signal is delayed by free electrons and air density as it propagates through the troposphere. The refractivity ($N$) of the troposphere can be expressed as in Thayer (1974):

$$N = 10^6(n - 1) \quad [3.4]$$

where n denotes the refractive index. The tropospheric refractivity can be split into hydrostatic ($N_{dry}$) and wet components ($N_{wet}$), and can be related to meteorological parameters such as temperature, partial pressure of water vapour, and dry gases as formulated in Hofmann-Wellenhof et al. (2008):

$$\left.\begin{aligned} N &= N_{dry} + N_{wet} \\ &= k_1.\frac{p-e}{T} + k_2.\frac{e}{T} + k_3.\frac{e}{T^2} \end{aligned}\right\} \quad [3.5]$$

with

$$\left.\begin{aligned} k_1 &= (77.604 \pm 0.014) K\ mbar^{-1} \\ k_2 &= (64.79 \pm 0.08) K\ mbar^{-1} \\ k_2 &= (3.776 \pm 0.004) 10^5 K^2\ mbar^{-1} \end{aligned}\right\} \quad [3.6]$$

where $T$ denotes temperature in degrees Kelvin ($K$); $p$ denotes the partial pressure of dry gases in millibars (mbar); $e$ denotes the partial pressure of water vapour in mbar; and $k_i$ (i=1,2,3) denotes the empirical constants as determined by Thayer (1974).

### *2.2.1. Estimation of Zenith Tropospheric Delay*

The troposphere delays the signal and can be described as an integral to $N$ in the zenith path ($z$) from satellite $s$ to receiver $r$ as:

$$\triangle = 10^{-6} \int_r^s N dz \quad [3.7]$$

where $\triangle$ denotes the signal delay. Therefore, the integrals of $N$ in the zenith direction are referred to as the ZWD and ZHD. Substituting the integrals of $N$ in [3.7] leads to

$$\triangle = 10^{-6} \int_r^s N_{dry} dz + 10^{-6} \int_r^s N_{wet} dz \quad [3.8]$$

Depending on the satellite elevation angle, the total tropospheric delay in the slant path can be mapped to the zenith direction. Taking the mapping function into account, [3.7] can be expressed in terms of ZWD and ZHD with respect to the satellite elevation angle ($E$) as

$$\triangle = ZWD.(m_w.E) + ZHD.(m_h.E) \quad [3.9]$$

where $m_w$ and $m_h$ denote the wet and hydrostatic mapping functions, respectively. Thus, having mapped tropospheric delay to the zenith direction, the ZTD parameter is readily estimated as an integral, as in Wilgan et al., (2017):

$$ZTD = 10^{-6}\int_z Ndz \quad [3.10]$$

Also known as the zenith total delay (ZTD), the ZTD is related to $N$ of the troposphere as indicated in [3.10].

### *2.2.2. Estimation of Zenith Hydrostatic Delay*

While the ZTD can be estimated as integral [3.10], the ZHD can also be extracted from it by using the Saastamoinen model (Saastamoinen, 1972) as expressed in Davis et al. (1985):

$$ZHD = \frac{0.0022768\text{m/hPa}p}{1 - 0.00266\,cos(2\phi) - 2.8.10^{-7}m^{-1}h}\Big\} \quad [3.11]$$

where $p$ denotes the surface pressure observed at the receiver position; $\phi$ denotes the station latitude in radians; $h$ denotes the orthometric height in kilometres. The ZWD has a poor predictive characteristic as compared to the ZHD (Bevis et al., 1992). Since the ZTD is simply the sum of ZWD and ZHD, the modelled ZHD in [2.11] is used to estimate ZWD:

$$ZWD = ZTD - ZHD \quad [3.12]$$

## 3. Characteristics of the Malawi CORS Network

### 3.1. Decommissioned CORS Network

Malawi briefly recorded GPS single-frequency observations from CORS monuments between March and May in 1997 in five different geographical locations. In all the five stations, GPS observations were logged using a TRIMBLE 4000SSI geodetic receiver equipped with a TRM29659.00 antenna. Operated by the East Africa 1997 campaign, the average data recording periods for the receivers are summarized from initial to the final day of year (DOY) in Table 1.

Table 1: Initial CORS monuments in Malawi.

| Monument | Recording Period From -To | Latitude | Longitude | Height [m] | Location Remarks |
|---|---|---|---|---|---|
| BND1 | DOY: 103-104 | -11° 55' 18.84" | 34° 10' 44.04" | 531.4 | Lake Malawi, Nkhata-Bay |
| EPH1 | DOY: 111-113 | -12° 10' 33.60" | 33° 27' 54" | 1292.5 | Embangweni, Mzimba District |
| LIV1 | DOY: 116-117 | -10° 35' 42.36" | 34° 6' 23.76" | 1305.3 | Livingstonia, Rumphi District |
| MAP1 | DOY: 090-092 | -12° 6' 34.56" | 33° 38' 30.12" | 1646.8 | Hill Top, Mzimba District |
| NKB1 | DOY: 126-127 | -11° 37' 0.12" | 34° 17' 0.60" | 532.8 | Nkhata-Bay District |

Since the initial campaign, another CORS station has been installed in Malawi in 2008 by the Department of Land Surveys and funded by Hartebeesthoek Radio Astronomy Observatory (HartRAO) Space Geodesy Programme of South Africa. The CORS was installed at the top of the Home Affairs and Department of Human Resources building (Capitol Hill) in Lilongwe City (AFREF, 2008). This station (not included in Table 1) was specifically installed as part of African Reference Frame (AFREF) to support satellite positioning by GPS in Malawi. In this paper, the CORS stations that were constructed in 1997 have been termed "decommissioned CORS" (refer to Figure 1).

### 3.2. Operational CORS Network

Recently, a new CORS network has been initiated by the Malawi Rifting GPS Network (MRGN) and the Africa Array GPS Network (AAGN) in Malawi. Currently, Malawi has six operational CORS monuments. Four of the CORS (Livingstonia, Vwaza Marsh, Karonga, and Chitipa) are operated by MRGN, and the other two (Mzuzu and Zomba) are operated by AAGN. The station characteristics for the operational CORS network in Malawi are summarized in Table 2. Figure 1 depicts the distribution of the CORS network in Malawi.

Table 2: Station characteristics for Malawi CORS network.

| **Monument** | **Livingstonia** | **Mzuzu** | **Karonga Airport** | **Chitipa** | **Vwaza Marsh** | **Zomba** |
|---|---|---|---|---|---|---|
| Marker | LIVA | MZUZ | KARO | CPTM | VWZM | ZOMB |
| Latitude | -10° 36' 49.32" | -11° 25' 30.36" | -9° 57' 14.76" | -9° 42' 4.68" | -11° 10' 31.08" | -15° 22' 32.88" |
| Longitude | 34° 06' 25.56" | 34° 00' 21.24" | 33° 53' 43.80" | 33° 15' 46.80" | 33° 34' 27.84" | 35° 19' 30.36" |
| Height | 1359.50 m | 1261.24 m | 513.80 m | 1285.60 m | 1113.30 m | 972.63 m |
| Receiver | TRIMBLE NETR9 | TRIMBLE NETR8 | TRIMBLE NETR8 | TRIMBLE NETR8 | TRIMBLE NETR8 | TRIMBLE NETRS |
| Antenna | TRM57971.00 | TRM59800.00 | TRM57971.00 | TRM57971.00 | TRM57971.00 | TRM59800.00 |

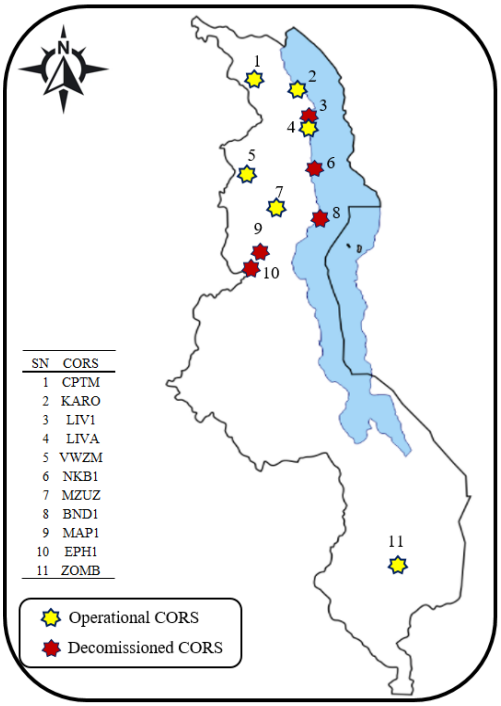


Figure 1: Distribution of CORS monuments in Malawi.

## 4. Experimental Datasets and Processing

The GNSS datasets for the stations used in this paper (Table 2) were obtained from the University NAVSTAR Consortium (UNAVCO) at https://www.unavco.org/. UNAVCO is sponsored by the National Science Foundation (NSF) and the National Aeronautics and Space Administration (NASA) to provide free services to support research worldwide. In order to test the Malawi CORS network on GNSS meteorology, ten days of GNSS observations spanning from DOY 001 to DOY 010 in 2016 were downloaded from UNAVCO. Due to data unavailability in the first constructed CORS monuments, only the geodetic stations in Table 2 were considered.

All the necessary PPP corrections according to Kouba (2009) were applied. The processing parameters are summarized in Table 3. The ZTD was estimated using Equation [3.10] whereas the ZHD was modeled using [3.11]. The water vapour refractivity is responsible for most of the wet delay and it was estimated using [2.12]. The estimated quantities of ZTD, ZHD, and ZWD for the selected days were compared. Finally, the standard deviation was used to express the positioning repeatability of the CORS monuments.

Table 3: Summary of the processing scheme.

| Parameter | Setting |
|---|---|
| Observable | IF code and phase, Equation [2.1] |
| GNSS Datasets | GPS constellation |
| Frequency | GPS L1 and L2 |
| Elevation Mask (Cut-off) | 7 º |
| Sampling Interval | 15 Seconds |
| Orbits and Clocks | IGS Final (300 seconds) |
| Satellite Phase Center Offset (PCO) | igs14.atx |
| Satellite Phase Center Variation (PCV) | igs14.atx |
| Receiver Phase Center Offset (PCO) | igs14.atx |
| Receiver Phase Center Offset (PCV) | igs14.atx |
| Tropospheric Mapping Function | Vienna Mapping Function (Boehm et al., 2006a) |
| Zenith Hydrostatic Delay (ZHD) | Saastamoinen, Equation [3.11] |
| Zenith Wet Delay (ZWD) | Global Mapping Function (Boehm et al., 2006b) |
| Weighting Scheme | Elevation-dependent |
| Phase wind-up | Corrected (Wu et al., 1992) |
| Relativistic effect | Applied with respect to the IERS convention 2010 (Kouba, 2009) |

# 5. Results and Discussion

## 5.1. The Estimated ZTD

Using GPS datasets for ten days (DOY 001-010) of the year 2016, the ZTDs were estimated for the Malawi CORS network. Figure 2 depicts the ZTD-PPP derived time series for CTPM, KARO, LIVA, MZUZ, VWZM, and ZOMB CORS monuments.

As can be seen from Figure 2, the estimated ZTDs for CTPM, LIVA, MZUZ, VWZM and ZOMB are consistent and within the same range of approximately 212 cm to 232 cm. However, KARO has the maximum estimated ZTD, reaching up to 250 cm on average. For the selected 10 days, the highest total delay for KARO is attributed to the large contribution of the ZHD (Table 4). The highest ZTD for 10 days simply indicates the high refractivity of dry gases in the troposphere for the KARO station. This is, on the other hand, caused by an increase in average atmospheric pressure, as demonstrated in Figure 2, reaching up to 950 mbars.

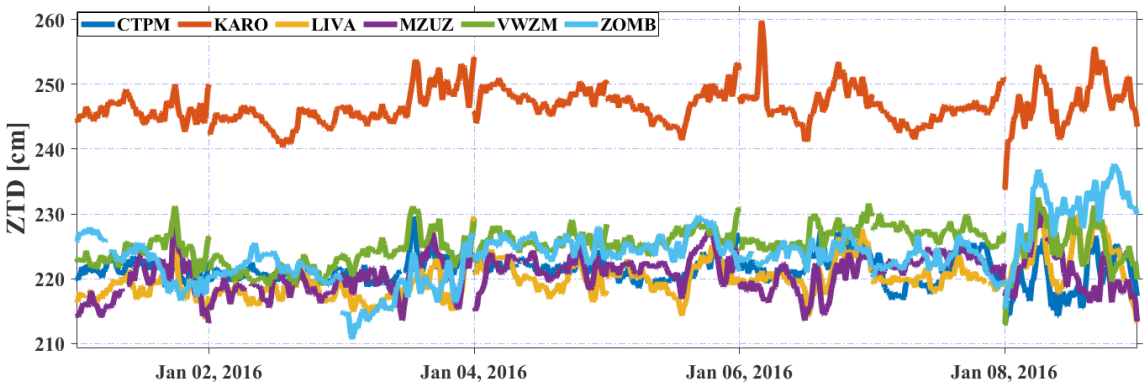


Figure 2: Comparison of estimated ZTD time series for the selected days.

## 5.2. The Estimated ZWD

The ZWD was derived from the difference between ZTD and ZHD and the associated time series for the estimated ZWD are shown in Figure 3 and the computed numerical values are presented in Table 4. From Table 4, it can be demonstrated that ZHD contributes to almost 90% of the total delay. This is evident from the numerical values between ZWD and ZHD. To better distinguish between the variations in the estimated meteorological parameters, the mean ZTD, ZWD and ZHD is illustrated in Figure 3. What is apparent is that ZOMB has the minimum ZWD of about 34 cm. This can also be verified from Table 4 and the least wet delay may be attributed to a higher influence of water vapour refractivity in the troposphere (Yuan et al., 2019). This can be explained better by comparing water vapour refractivity with the average atmospheric pressure of about 903 mbar for the selected days (Figure 4). On the other hand, LIVA CORS has the least atmospheric pressure, namely only about 864 mbars (Figure 5).

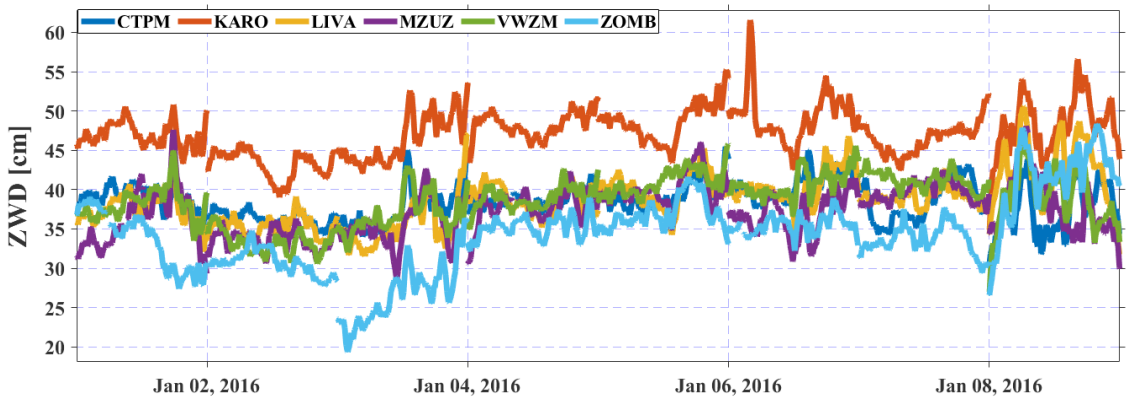


Figure 3: Comparison of estimated ZWD time series for the selected days.

Table 4: Comparison of estimated ZTD, ZWD and ZHD from GPS observations.

| CORS | ZTD [cm] | ZWD [cm] | ZHD [cm] |
|---|---|---|---|
| LIVA | 220.04 | 38.65 | 181.40 |
| MZUZ | 220.67 | 37.23 | 183.44 |
| KARO | 246.68 | 47.19 | 199.49 |
| CTPM | 221.35 | 38.43 | 182.92 |
| ZOMB | 223.77 | 34.27 | 189.50 |
| VWZM | 225.18 | 38.66 | 186.52 |
| Max | 246.68 | 47.19 | 199.49 |
| Min | 220.04 | 34.27 | 181.40 |

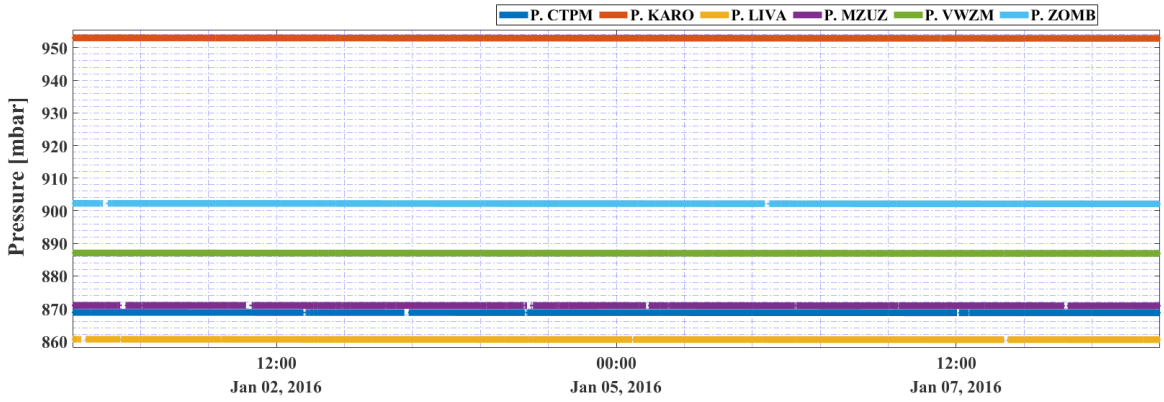


Figure 4: Pressure as estimated from GPS observations from Malawi CORS.

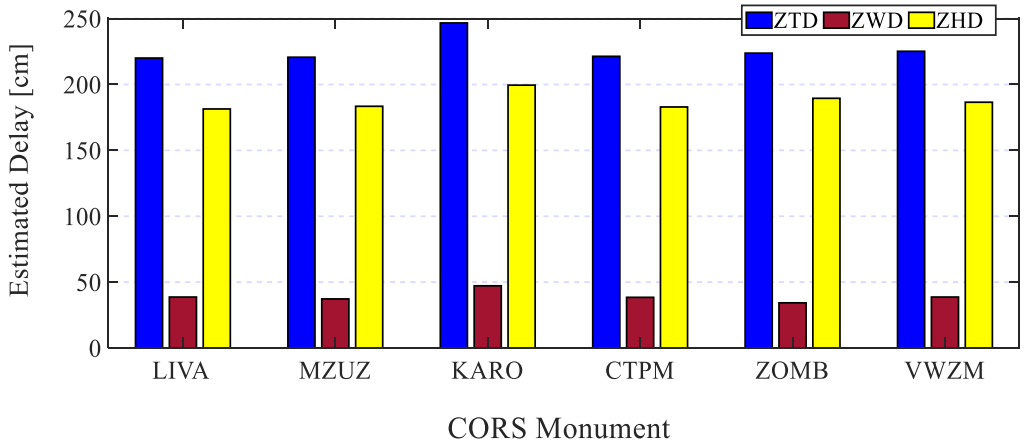


Figure 5: Estimated ZTD, ZWD and ZHD from GPS observations.

### 5.3. Positioning Performance

In situations where the visible number of satellites is small, the overall positioning performance declines. For the determination of the ZTD described above, knowledge about the tracked satellite vehicles (SVs) at each CORS is thus necessary. Hence, for the selected days in this study, the visible SVs are illustrated in Figure 5. As can be noticed from Figure 6, at least ten GPS satellites were observed on all the selected days. As indicated in Suya (2019), this number of tracked satellites is more than enough for the estimation of parameters by PPP.

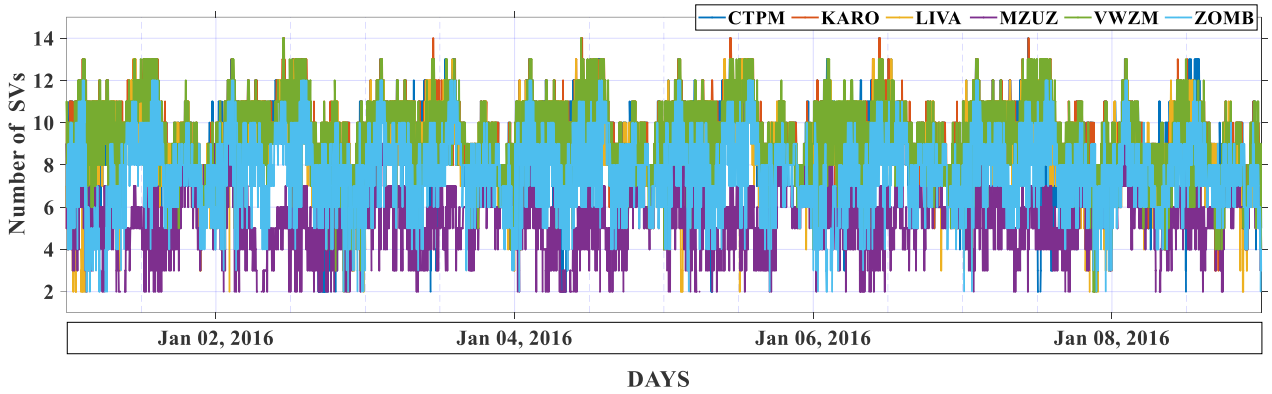


Figure 6: Average number of observed satellites at the CORS stations.

To assess the effect of the estimated ZTD on positioning performance, the positional stability of the CORS stations during the sampled period was examined. This was performed by computing the standard deviations between the estimated coordinates and the *a priori* coordinates. The estimated coordinates and their associated standard deviations that express the CORS 3D positioning repeatability for the six stations are presented in Table 5. The geodetic coordinates in Table 5 are referenced to the local geodetic datum of the World Geodetic System 1984 (WGS – 84).

Moreover, the standard deviations in latitude, longitude, and ellipsoidal height have been expressed as $\sigma_{Lat}$, $\sigma_{Long}$, and $\sigma_{Elev}$, respectively. The standard deviations for the positioning repeatability in Table 5 were computed at a 95% confidence interval and have been expressed in centimetre for convenience and plotted in Figure 6. The positioning repeatabilities demonstrate obvious variability in the station coordinates, especially in the height dimension. For the Mzuzu station, the standard deviation in the height component can reach as high as 1.49 cm. From Figure 7, there is no obvious difference in the standard deviations for latitude and longitude except for Mzuzu CORS. Based on the selected days, the positioning performance in all the dimensions may satisfy geodynamics studies. Considering the number of days investigated in this study, these repeatabilities are insignificant.

Table 5: Averaged coordinates for the stations.

| | LIVA | MZUZ | KARO | CTPM | VWZM | ZOMB |
|---|---|---|---|---|---|---|
| Latitude | -10° 36' 49.32" | -11° 25' 30.36" | -9° 57' 14.76" | -9° 42' 04.68" | -11° 10' 31.08" | -15° 22' 32.88" |
| | -10° 36' 49.3981" | -11° 25' 30.3488" | -9° 57' 14.9230" | -9° 42' 04.7836" | -11° 10' 31.0985" | -15° 22' 33.0268" |
| $\sigma_{Lat}$ | ± 0.002 m | ± 0.003 m | ± 0.002 m | ± 0.002 m | ± 0.002 m | ± 0.002 m |
| Longitude | 34° 06' 25.56" | 34° 00' 21.24" | 33° 53' 43.80" | 33° 15' 46.80" | 33° 34' 27.84" | 35° 19' 30.36" |
| | 34° 06' 25.3948" | 34° 00' 21.4142" | 33° 53' 43.6944" | 33° 15' 46.8008" | 33° 34' 27.9871" | 35° 19' 30.4878" |
| $\sigma_{Long}$ | ± 0.005 m | ± 0.007 m | ± 0.005 m | ± 0.005 m | ± 0.005 m | ± 0.005 m |
| Height [m] | 1359.500 | 1261.240 | 513.800 | 1285.600 | 1113.300 | 972.630 |
| | 1359.552 | 1261.219 | 513.838 | 1285.54 | 1113.312 | 972.627 |
| $\sigma_{Elev}$ | ± 0.011 m | ± 0.015 m | ± 0.009 m | ± 0.010 m | ± 0.009 m | ± 0.012 m |

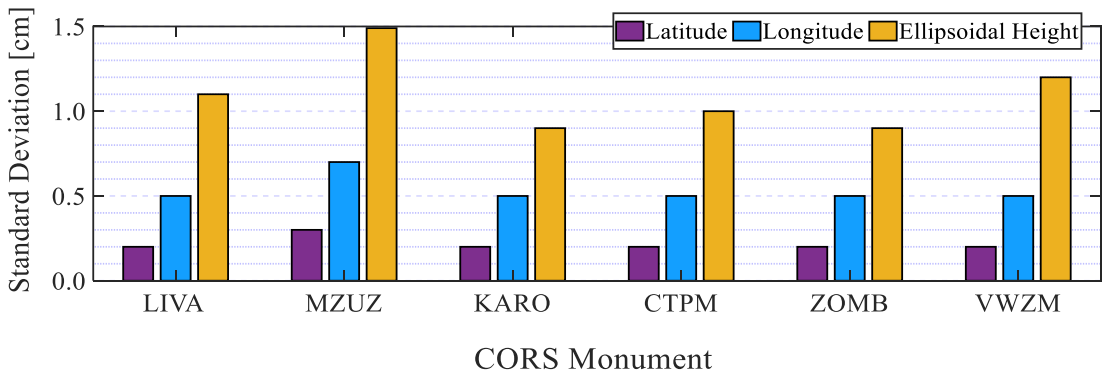


Figure 7: Standard deviations for the estimated positions.

## 6. Conclusions

Malawi CORS are commonly used for geophysical and geodynamics studies. This paper attempted to estimate the meteorological parameters from the operational CORS network using the PPP technique. Ten days of GNSS datasets from DOY 001 to 010 in 2016 were used to estimate the ZTD, ZWD, and ZHD, including coordinate repeatabilities for the six CORS monuments. Results indicate that the mean ZTD, ZWD, and ZHD can reach as high as 247cm, 47 cm, and 199 cm at the Karonga CORS monument, respectively. This was attributed to the high atmospheric pressure of about 903 mbars for the experimented days. On the other hand, the minimum ZTD, ZWD and ZHD for the stations can drop to as low as 220 mm, 24 mm, and 181 mm at the Livingstonia CORS monument,

respectively. The reduced values were attributed to low pressure at the Livingstonia CORS monument. The study also indicates that the ZHD contributes to more than 90% of the total delay in the stations. In the case of positioning performance, there was no obvious disparity in the latitude (less than 0.5 cm), longitude (less than 1 cm), and ellipsoidal height repeatabilities (less than 1.5 cm). Therefore, the results clearly demonstrate that the Malawi CORS network may be used for GNSS-based meteorological applications using the available geodetic receivers. This study used datasets for a few days to fully quantify the meteorological parameters. Therefore, a similar study may be conducted with datasets spanning the whole period of a year or more. Furthermore, for high precision meteorological applications, Malawi may consider densifying the available network with geodetic grade receivers for the robust estimation of meteorological parameters.

## 7. Acknowledgement

The authors gratefully acknowledge UNAVCO for the CORS GNSS observation datasets used in this project. The satellite clocks, orbits, and all other PPP datasets were retrieved from the IGS (http://www.igs.org/).

## 8. References

AFREF 2008 'African Geodetic Reference Frame (AFREF)-Newsletter', *Malawi First Continuous Operating Reference GPS Station Established*. Retrieved from: https://kb.unavco.org/kb/file.php?id=757

Ahmed, F., Václavovic, P., Teferle, F. N., Douša, J., Bingley, R., & Laurichesse, D. 2016. Comparative analysis of real-time precise point positioning zenith total delay estimates. *GPS Solutions*. no. 20, pp. 187–199. Retrieved from: https://doi.org/10.1007/s10291-014-0427-z

Alshawaf, F., Balidakis, K., Dick, G., Heise, S., & Wickert, J. 2017 'Estimating trends in atmospheric water vapor and temperature time series over Germany', *Atmospheric Measurement* Techniques 10, pp. 3117–3132. https://doi.org/10.5194/amt-10-3117-2017

Awange, J. L. 2011 'Environmental Monitoring using GNSS: Global Navigation Satellite Systems', *Environmental Science and Engineering*. Springer, Berlin, Heidelberg

Balidakis, K., Nilsson, T., Zus, F., Glaser, S., Heinkelmann, R., Deng, Z., & Schuh, H. 2018 'Estimating Integrated Water Vapor Trends from VLBI, GPS, and Numerical Weather Models: Sensitivity to Tropospheric Parameterization', *Journal of Geophysical Research: Atmospheres*. vol. 123, no. 12. https://doi.org/10.1029/2017JD028049

Bevis, M., Businger, S., Herring, T. A., Rocken, C., Anthes, R. A., & Ware, R. H 1992 'GPS meteorology: remote sensing of atmospheric water vapor using the global positioning system', *Journal of Geophysical Research*. vol. 97, no D14. https://doi.org/10.1029/92jd01517

Bock, O., Willis, P., Lacarra, M., & Bosser, P. 2010 'An inter-comparison of zenith tropospheric delays derived from DORIS and GPS data', *Advances in Space Research*. vol. 46, no 12, pp. 1648-1660. https://doi.org/10.1016/j.asr.2010.05.018

Boehm, J., Niell, A., Tregoning, P., & Schuh, H. 2006 'Global Mapping Function (GMF): A new empirical mapping function based on numerical weather model data', *Geophysical Research Letters*. vol. 33, no. 7. https://doi.org/10.1029/2005GL025546

Boehm, J., Werl, B. and Schuh, H. 2006 'Troposphere mapping functions for GPS and very long baseline interferometry from European Centre for Medium-Range Weather Forecasts operational analysis data', *Journal of Geophysical Research: Solid Earth*. vol. 111, no B2.

Davis, J. L., Herring, T. A., Shapiro, I. I., Rogers, A. E. E., & Elgered, G. 1985 'Geodesy by radio interferometry: Effects of atmospheric modeling errors on estimates of baseline length', *Radio Science*. vol. 20, no. 6, pp. 1593-1607. https://doi.org/10.1029/RS020i006p01593

Essen, L. and Froome, K. D. 1951 'Dielectric constant and refractive index of air and its principal constituents at 24,000 Mc./s.', *Nature*. B 64 862.

Gutman, S. I., Sahm, S. R., Benjamin, S. G., Schwartz, B. E., Holub, K. L., Stewart, J. Q., & Smith, T. L. 2004 'Rapid retrieval and assimilation of ground-based GPS precipitable water observations at the NOAA Forecast Systems Laboratory: Impact on weather forecasts', *Journal of the Meteorological Society of Japan*. vol. 82, no. 1B. https://doi.org/10.2151/jmsj.2004.351

Gutman, S. I. and Benjamin, S. G. 2001 'The Role of Ground-based GPS Meteorological Observations in Numerical Weather Prediction', *GPS Solutions*. no. 4, pp. 16-20.

Heinkelmann, Boehm, J., Schuh, H., Bolotin, S., Engelhardt, G., MacMillan, D. S., Negusini, M., Skurikhina, E., Tesmer, V., & Titov, O. 2007 'Combination of long time-series of troposphere zenith delays observed by VLBI', *Journal of Geodesy*. no. 81, pp. 483–501. https://doi.org/10.1007/s00190-007-0147-z

Hofmann-Wellenhof, B., Lichtenegger, H. and Wasle, E. 2008 *GNSS – Global Navigation Satellite Systems - GPS, GLONASS, Galileo, and more*, *Applied Sciences*. Springer, Berlin, Germany.

Hurter, F. and Maier, O. 2013 'Tropospheric profiles of wet refractivity and humidity from the combination of remote sensing data sets and measurements on the ground', *Atmospheric Measurement Techniques*, vol. 6. no. 11, pp. 3083–3098.

Kiyani, A., Shah, M., Ahmed, A., Shah, H. H., Hameed, S., Adil, M. A., & Naqvi, N. A. 2020 'Seismo ionospheric anomalies possibly associated with the 2018 Mw 8.2 Fiji earthquake detected with GNSS TEC', *Journal of Geodynamics*. doi:10.1016/j.jog.2020.101782.

Kouba, J. 2009 'A Guide to using international GNSS Service ( IGS ) Products', *Geodetic Survey Division: Natural Resources. Canada, Ottawa,* no. 6, p. 34., Retrieved from: <http://acc.igs.org/UsingIGSProductsVer21.pdf>. Viewed: 11 December 2018.

Krietemeyer, A., ten Veldhuis, M. C., van der Marel, H., Realini, E., & van de Giesen, N. 2018 'Potential of cost-efficient single frequency GNSS receivers for water vapor monitoring', *Remote Sensing*. vol.10, no. 9. https://doi.org/10.3390/rs10091493

Leick, A, Rapoport, L, & Tatarnikov, D 2015, GPS Satellite Surveying, 4th edition, Wiley, USA.

Paziewski, J. 2020 'Recent advances and perspectives for positioning and applications with smartphone GNSS observations', *Measurement Science and Technology*. vol.31, no. 9.

Pesyna, K. M., Heath, R. W. and Humphreys, T. E. 2014 'Centimeter positioning with a smartphone-Quality GNSS antenna', in *27th International Technical Meeting of the Satellite Division of the Institute of Navigation, ION GNSS 2014*. pp. 1568-1577.

Pollet, A., Coulot, D., Bock, O., & Nahmani, S. 2014 'Comparison of individual and combined zenith tropospheric delay estimations during CONT08 campaign', *Journal of Geodesy*. no. 88, pp.1095–1112 doi: 10.1007/s00190-014-0745-5.

Rahimi, Z., Mohd Shafri, H. Z. and Norman, M. 2018 'A GNSS-based weather forecasting approach using Nonlinear Auto Regressive Approach with Exogenous Input (NARX)', *Journal of Atmospheric and Solar-Terrestrial Physics*. no. 178, pp. 74-84.

Saastamoinen, J. 1972 'Contributions to the theory of atmospheric refraction', *Bulletin Géodésique*. no. 107, pp. 13–34.

Shillington, D. J., Gaherty, J. B., Ebinger, C. J., Scholz, C. A., Selway, K., Nyblade, A. A., … Moshi, M. 2016 'Acquisition of a unique onshore/offshore geophysical and geochemical dataset in the northern Malawi (Nyasa) rift', *Seismological Research Letters*. vol. 87, no. 6, pp. 1406–1416. https://doi.org/10.1785/0220160112

Shoji, Y. 2009 'A study of near real-time water vapor analysis using a nationwide dense GPS network of Japan', *Journal of the Meteorological Society of Japan*. vol. 87, no. 1, pp.1-18.

Suya, R. G. 2019 'Static precise point positioning using triple-constellation GNSS', *My Coordinates. vol. 15, no. 7*, pp. 32. Retrieved from: https://mycoordinates.org/static-precise-point-positioning-using-triple-constellation-gnss/.

Teke, K., Nilsson, T., Böhm, J., Hobiger, T., Steigenberger, P., García-Espada, S., … Willis, P. 2013 'Troposphere delays from space geodetic techniques, water vapor radiometers, and numerical weather models over a series of continuous VLBI campaigns', *Journal of Geodesy*. no. 87, pp. 981–1001. https://doi.org/10.1007/s00190-013-0662-z

Thayer, G. D. 1974 'An improved equation for the radio refractive index of air', Radio Science. vol. 9, no. 10, pp. 803–807. https://doi.org/10.1029/RS009i010p00803

Uradziński, M. and Bakuła, M. 2020 'Assessment of static positioning accuracy using low-cost smartphone GPS devices for geodetic survey points' determination and monitoring', Applied Sciences (Switzerland). vol. 10, no. 15.

Wilgan, K., Hurter, F., Geiger, A., Rohm, W., & Bosy, J. 2017 'Tropospheric refractivity and zenith path delays from least-squares collocation of meteorological and GNSS data', *Journal of Geodesy*, vol. 91, no. 2, pp. 117–134. https://doi.org/10.1007/s00190-016-0942-5

Wu, J. T., Wu, S. C., Hajj, G. A., Bertiger, W. I., & Lichten, S. M. 1992 'Effects of antenna orientation on GPS carrier phase', in *Advances in the Astronautical Sciences*. pp. 1647-1660.

Yuan, Y., Holden, L., Kealy, A., Choy, S., & Hordyniec, P. 2019 'Assessment of forecast Vienna Mapping Function 1 for real-time tropospheric delay modeling in GNSS', *Journal of Geodesy*. no. 93, pp. 1501–1514. https://doi.org/10.1007/s00190-019-01263-9

Zhao, Q., Yao, Y., Yao, W., & Li, Z. 2018 'Real-time precise point positioning-based zenith tropospheric delay for precipitation forecasting', *Scientific Reports*. no.7939.

Zhao, Q., Yao, Y. and Yao, W. 2018 'Troposphere water vapour tomography: A horizontal parameterised approach', *Remote Sensing*. vol. 10, no. 8. https://doi.org/10.1038/s41598-018-26299-3

Zumberge, J. F., Heflin, M. B., Jefferson, D. C., Watkins, M. M., & Webb, F. H. 1997 'Precise point positioning for the efficient and robust analysis of GPS data from large networks, *Journal of Geophysical Research: Solid Earth*. Vol. 102, no. B3, pp. 5005–5017. https://doi.org/10.1029/96JB03860